Measurements of the Directional Spectra of Shallow Water Waves Using the Maximum Entropy Principle and a Single Ocean Bottom Seismometer

TOM NYE, TOKUO YAMAMOTO AND MARK TREVORROW

Division of Applied Marine Physics, Rosenstiel School of Marine and Atmospheric Science, University of Miami, Miami, Florida

15 August 1989 and 13 April 1990

ABSTRACT

A new method for measurement of the directional spectra of surface gravity (water) waves is presented here. Measurements are made at a single point by orthogonally mounted seismometers buried 0.5 meters below the seabed surface and a pressure sensor resting on the seafloor. The maximum entropy principle, which uses entropy as an index of uncertainty in the directional distribution, is used to find the directional distribution function for the waves traveling through the sediments as measured by the seismometers. This function is combined with the frequency spectra of the ocean surface waves to form the directional spectra of the surface gravity waves. Single point measurements are advantageous due to the relative ease of implementation and expense compared to arrays, as well as for measurement of non-uniform wave fields. Due to attenuation of shorter wavelengths with depth, this procedure is limited to shallow or intermediate depths. Field data was collected on the New Jersey Shelf and the results show that the method produced high directional resolution for instruments that were adequately coupled with the seabed.

1. Introduction

Estimates of the energy density of ocean surface waves as a function of wave frequency and wave propagation direction (directional spectra estimates), are essential to many aspects of ocean and coastal engineering. Directional spectra are used in the design and analysis of moorings, piles, and offshore towers, in the prediction of ship response, for wave forecasting and hindcasting, and in the study of sediment transport and pollution control.

Many methods for measuring directional spectra have been proposed. Remote sensing by light or radio waves is possible. More often, direct in situ measurements are used. These can be from a horizontal array of instruments measuring one wave property, or from a single instrument package measuring three or more wave properties, first proposed by Longuet-Higgins et al. (1963).

Arrays can be difficult to implement. If the array spacing is larger than one-half wavelength of the frequency being analyzed, spatial aliasing occurs. When the spacing is small, the long-wave estimates tend to be smeared due to noise according to Jefferys (1982). Therefore, there is a need for many instruments of variable spacing for good resolution without aliasing. Special configurations such as star arrays are used to minimize the number of instruments while maintaining acceptable resolution (Goda 1983). Also, convolution with data adaptive windows such as is the case with the Maximum Likelihood Method (MLM) developed by Capon (1983), are used to improve resolution. Hashimoto et al. (1987) recently used a Bayesian approach to estimate directional spectra for use with wave records consisting of at least four elements of wave properties. The Bayesian approach, originally proposed by Akaike (1980), is capable of high resolution even when the cross-power spectra are contaminated with estimation errors. This model showed better resolution for various numerical and field tests than MLM, but cannot be used for a three element wave record. Observation at a single point (a three element wave record) is useful for ease of implementation and expense compared to arrays, as well as for measurement of nonuniform wave fields characterized by refraction and diffraction.

Longuet-Higgins' method for a single point uses a non-negative smoothing function to weight the Fourier series coefficients, which removes the negative sidelobes but produces poor resolution. The resolution can be improved by increasing the number of quantities measured. Use of a cloverleaf buoy proposed by Mitsuyasu (1975), for example, increases the number of measured wave properties and therefore achieves improved resolution. Another way to improve resolution is to fit an assumed directional spreading function to the measured one. However, if the assumed function is independent of the data, the estimate may be biased if the true spectrum is different (Kobune and Hashimoto 1986). Data adaptive models such as MLM, extended

Corresponding author address: Thomas Nye, RSMAS-AMP, 4600 Rickenbacker Causeway, Miami, Florida 33149.

for this purpose by Isobe (1984), and the Maximum Entropy Principle model developed by Kobune and Hashimoto (1986) can be used to remove this bias. These do not have fixed window functions associated with them and therefore can adjust to the true spectrum.

The Maximum Entropy Method (MEM), first introduced by Burg (1967), was used as a nonlinear spectral estimation for a time series. He proposed that instead of using zero for covariance values outside of the data record, one could use artificial covariance values based on information content (maximizing entropy) to increase resolution (McDonough 1983). Lacoss (1971), comparing MLM to MEM, found MEM to have better resolution. He also showed that both MLM and MEM produced the true spectrum for a simulated broad spectrum.

Kobune and Hashimoto (1986), recognized that the directional spreading function had the same properties as a joint probability distribution function and therefore information theory could be used to estimate the spreading function. The cross-spectral values are found by direct Fourier transform, after which the maximum entropy principle is applied to find the directional spread. Borgman (1985) has also outlined the use of data adaptive methods to analyze the wavenumber data after transformation to the frequency domain by a discrete Fourier transform.

This paper uses the maximum entropy model proposed by Kobune and Hashimoto (1986), but with data collected from an ocean bottom seismometer and a pressure sensor in shallow water. Until now, single-point data has been collected using the pitch–roll buoy (measures water surface elevation and two orthogonal components of surface slope), the cloverleaf buoy (measures same as well as three components of water surface curvature), or by current meters with a pressure sensor to measure orbital velocities and water surface elevation (Panicker 1974). Also, to measure velocity gradients, three current meters have been employed close together by Simpson (1969). Buoys are subject to large nonlinear motions (caused by their not being fixed relative to the waves) and to flipping over in heavy seas. Current meters need to be moored or fixed to a structure, which limits their usefulness and may also effect the wave field being measured.

This paper uses the assumption that the seabed motion is coupled to the traveling surface gravity waves due to pressure fluctuations (Yamamoto et al. 1978, 1986; Trevorrow et al. 1989a,b). The directional spreading function can be found for the sediment waves using horizontal seabed accelerations and then combined with the frequency spectra of the surface waves as measured from hydrodynamic pressure to form the directional spectra.

A series of experiments have been conducted in July 1988 off the coast of New Jersey. The purpose of these experiments was to test a Bottom Shear Modulus Profiler (BSMP) system (see Trevorrow et al. 1988; Yamamoto et al. 1989). Fortunately, the Ocean Bottom Seismometer data collected was also well suited for use with the Maximum Entropy Principle directional spectra estimation method (MEPOBS). The extended MLM is also tested for comparison purposes. The sole purpose of this note is to present this new method for measuring directional spectra using the data collected for the BSMP system. Comparisons with other methods of measurement and analysis will be done in the future to assess the practicality of this method.

2. Theory

The following derivation is similar to the derivation by Isobe (1984), with additions to allow for ocean bottom measurements.

For small wave amplitude, the water surface elevation η, at a point $\mathbf{x} = (x, y)$ and a time t, can be expressed as:

$$\eta(\mathbf{x}, t) = \int_f \int_{\mathbf{k}} \exp i(\mathbf{k}) \cdot \mathbf{x} - 2\pi f t) Z(d\mathbf{k}, df) d\mathbf{k} df \tag{1}$$

where f is the wave frequency, $\mathbf{k}$ is the wavenumber vector and Z is the complex wave amplitude. The wavenumber-frequency spectrum, $S(\mathbf{k}, f)$, may be defined as

$$S(\mathbf{k}, f) d\mathbf{k} df = \langle Z(d\mathbf{k}, df) Z^*(d\mathbf{k}, df) \rangle. \tag{2}$$

The symbol $\langle\ \rangle$ represents the ensemble spectral averaging and $*$ denotes the complex conjugate. The wavenumber vector, $\mathbf{k}$, is a function of wavenumber k and propagation direction θ. For surface waves, k is uniquely determined from f by the dispersion relation.

$$(2\pi f)^2 = gk \tanh(kd). \tag{3}$$

Since it assumed that the sediment waves and the surface gravity waves move together, this dispersion relation also holds for the sediment waves. All functions of $(\mathbf{k}, f)$ can now be expressed in terms of (f, θ), however, the integral will continue to be expressed in terms of $\mathbf{k}$ until $(\exp i\mathbf{k} \cdot \mathbf{x})$ is cancelled for simplicity.

For an arbitrary wave parameter $\xi_m(\mathbf{x}, t)$, equation (1) can be modified:

$$\xi_m(\mathbf{x}, t) = \int_f \int_{\mathbf{k}} H_m(f, \theta) \times \exp i(\mathbf{k} \cdot \mathbf{x} - 2\pi f t) Z(d\mathbf{k}, df) d\mathbf{k} df \tag{4}$$

where $H_m(f, \theta)$ is the transfer function:

$$H_m(f, \theta) = \cos^{\alpha_m}\theta \sin^{\beta_m}\theta h_m(f) \tag{5}$$

and $h_m(f)$ is the homogeneous transfer function to be discussed later. The α and β are positive integers such that $\alpha_m = 1$ if the wave parameter is measured in the x-direction, $\beta_m = 1$ if in the y-direction. Subscripts m

and n represent the mth and nth wave property; $\alpha_m + \alpha_n$ will be represented as α_{m+n}. The x-direction is arbitrarily aligned with one of the orthogonal, horizontally mounted seismometers which will be called the *radial* seismometer. Therefore, measurements of radial accelerations of bottom sediments are in the x-direction with $\theta \equiv 0$. Measurements made by the *transverse* seismometer are in the y-direction where $\theta = 90°$. Isobe shows that the cross-power spectrum $\Phi_{mn}(f)$ between two wave properties from (2) and (4) becomes

$$\Phi_{mn}(f) = \int_{\mathbf{k}} H_m(f, \theta) H_n^*(f, \theta) \times \exp[-i\mathbf{k}\cdot(\mathbf{x}_n - \mathbf{x}_m)] S(f, \theta) d\mathbf{k}. \quad (6)$$

Let

$$\phi_{mn}(f) = \frac{\Phi_{mn}(f)}{h_m(f) h_n^*(f)} \quad (7)$$

and

$$S(f, \theta) = S(f) G(\theta \,|f) \quad (8)$$

where $S(f)$ is the frequency spectrum of the surface waves and $G(\theta\,|f)$ is the directional spreading function of the waves measured by bottom accelerations and is a function of θ at each frequency f. Equation (6) now becomes

$$\frac{\phi_{mn}(f)}{S(f)} = \int_{\mathbf{k}} \cos^{\alpha_{m+n}}\theta \sin^{\beta_{m+n}}\theta G(\theta\,|f) \times \exp[-i\mathbf{k}\cdot(\mathbf{x}_m - \mathbf{x}_n)] d\mathbf{k} \quad (9)$$

where $\phi_{mn}(f)$ is the normalized cross-spectral matrix and is Hermitian. It can be divided into real and imaginary parts:

$$\phi_{mn}(f) = A_{mn}(f) - iB_{mn}(f). \quad (10)$$

Substituting into (9):

$$\frac{A_{mn}(f)}{S(f)} = \int_{\mathbf{k}} \cos^{\alpha_{m+n}}\theta \sin^{\beta_{m+n}}\theta G(\theta\,|f) \times \cos\mathbf{k}\cdot(\mathbf{x}_m - \mathbf{x}_n) d\mathbf{k}. \quad (11)$$

For a point observation, $\mathbf{x}_m = \mathbf{x}_n$, therefore (11) reduces to

$$\frac{A_{mn}(f)}{S(f)} = \int_0^{2\pi} \cos^{\alpha_{m+n}}\theta \sin^{\beta_{m+n}}\theta G(\theta\,|f) d\theta \quad (12)$$

and $B_{mn}(f) \equiv 0$.

The cross-power spectrum can be represented as

$$\Phi_{mn}(f) = C_{mn}(f) - iQ_{mn}(f) \quad (13)$$

where $C_{mn}(f)$ is the cospectrum and $Q_{mn}(f)$ is the quadrature spectrum. The coherence, $\gamma_{mn}(f)$, is defined by

$$\gamma_{mn}^2(f) = \frac{C_{mn}^2 + Q_{mn}^2}{C_{mm}C_{nn}}. \quad (14)$$

The coherence is a measure of data quality. For noise-free data, coherence should be 1.00. It should be noted that the coherence is not affected by the phase versus frequency response of the instruments. Now, from (7), $A_{mn}(f)$ becomes

$$A_{mn}(f) = \mathrm{Re}\left\{\frac{C_{mn}(f) - iQ_{mn}(f)}{h_m h_n^*}\right\}. \quad (15)$$

For m or n equal to 1, 2, 3; which represent pressure (measured at the bottom interface), radial, and transverse accelerations of the bottom sediments respectively; C_{12}, C_{13}, and Q_{23} are expected to be zero. The phase between horizontal accelerations and the pressure signal should be $\pm 90°$ and since phase ($\varphi = \arctan Q/C$), C_{12} and C_{13} must equal zero for noise-free data according to linear theory. Similarly, $\varphi_{23} = 180°$ or $360°$ and therefore $Q_{23} = 0$. The phase is affected by the phase versus frequency response of the instruments. Because the phase response information of the instruments are usually not exact, the phase between horizontal accelerations and the pressure signal may deviate from the theoretical values of $\pm 90°$. However, the coherence should not be affected by the instrument frequency response; therefore, the coherence is a more reliable indicator of data quality than the phase. This point will be discussed further when comparing real data.

Equation (12) can be rewritten in the form (Kobune and Hashimoto 1986):

$$\int_0^{2\pi} G(\theta\,|f) a_{mn}(\theta) d\theta = b_{mn} \quad (16)$$

where

$$b_{mn} = \frac{A_{mn}(f)}{S(f)}$$

and

$$a_{mn} = \cos^{\alpha_{m+n}}\theta \sin^{\beta_{m+n}}\theta.$$

Because seabed properties are not known exactly, linear wave theory cannot be used to calculate the transfer functions for the radial and transverse accelerations; therefore, measured values of the transfer function are used following the example of Isobe (1984).

$$h_1(f) = \frac{\rho g}{\cosh kd} \quad (17)$$

$$h_2(f) = h_3(f) = \left(|h_1|^2 \frac{C_{22} + C_{33}}{C_{11}}\right)^{1/2}. \quad (18)$$

The six Eqs. (15) can be simplified to five harmonics:

$$\int_0^{2\pi} G(\theta\,|f) a_j(\theta) d\theta = b_j \cdots, \quad \cdots j = 0, \cdots, 4 \quad (19)$$

$$a_0 = 1 \cdots, \quad \cdots b_0 = 1$$

$$a_1 = \cos\theta \cdots, \quad \cdots b_1 = \frac{-Q_{12}}{\sqrt{C_{11}(C_{22} + C_{33})}}$$

$$a_2 = \sin\theta \cdots, \quad \cdots b_2 = \frac{-Q_{13}}{\sqrt{C_{11}(C_{22} + C_{33})}}$$

$$a_3 = \cos 2\theta \cdots, \quad \cdots b_3 = \frac{C_{22} - C_{33}}{C_{22} + C_{33}}$$

$$a_4 = \sin 2\theta \cdots, \quad \cdots b_4 = \frac{2C_{23}}{C_{22} + C_{33}}. \tag{20}$$

Note that when $j = 0$ in (19), it simplifies to

$$\int_0^{2\pi} G(\theta \mid f)d\theta = 1. \tag{21}$$

It therefore behaves like a probability distribution function (pdf). One method in statistics of estimating a pdf is by maximizing the entropy. The information entropy, called Shannon's entropy, is defined by Hashimoto et al. (1987):

$$H = -\int_0^{2\pi} G(\theta \mid f) \ln[G(\theta \mid f)]d\theta. \tag{22}$$

The estimate $\hat{G}(\theta \mid f)$, which maximizes H, will be the best estimate of $G(\theta \mid f)$. $\hat{G}(\theta \mid f)$ can be found using Lagrange multipliers, λ, (22) and the constraint of (19) (Kobune and Hashimoto 1986).

$$\hat{G}(\theta \mid f) = \exp[-\lambda_0 - \sum_{j=1}^{4} \lambda_j a_j(\theta)]. \tag{23}$$

Substituting this into (19) yields

$$\int_0^{2\pi} (b_j - a_j(\theta)) \exp[-\sum_{l=1}^{4} \lambda_l a_l(\theta)]d\theta = 0 \tag{24}$$

$$j = 1, \cdots, 4$$

and,

$$\lambda_0 = \ln\left[\int_0^{2\pi} \exp(-\sum_{l=1}^{4} \lambda_l a_l(\theta))d\theta\right]. \tag{25}$$

This leaves four nonlinear equations to be solved numerically by a Newton-Raphson iteration scheme for the $\lambda_j, j = 1, \cdots, 4$. Once these are calculated, λ_0 can be found using (25). For most directional spreading functions, the solution converges rapidly with initial guesses of zero for the Lagrange multipliers. The solution is said to have converged when the difference between the multiplier values for the nth and the $(n + 1)$th iteration is less than 0.001. Smaller values have been used with no discernable change in the spreading function. For very narrow banded directional spectra, initial values of zero do not suffice and multipliers from neighboring frequencies which do show convergence are used as initial guesses.

The directional spectra of the surface waves is then estimated by multiplying the frequency spectra of the surface waves, $S(f)$, with the directional spreading estimate, $\hat{G}(\theta \mid f)$, calculated from (23).

3. Sea experiments

Data was collected in July 1988 at the Atlantic Generating Station (AGS) site near Atlantic City, New Jersey (Fig. 1). Typical water depth at the AGS site was 12 meters. An array of ocean bottom seismometers (OBSs) was deployed for use with the BSMP system. Units labeled 301 (39°28.24'N, 74°15.34'W) and 305 (39°28.18'N, 74°15.60'W) were chosen to test the MEPOBS system because the data collected showed that they were sufficiently coupled to the seabed with respect to horizontal motions. For a test of a single unit, it was necessary to check pressure to seismometer coherence, phase, and seismometer leveling to determine if the unit gave acceptable data before data collection began. If everything was not right, the instrument was pulled up, checked, and deployed again.

The success of this method relies on good coupling between the seismometers and the seabed sediments. Better coupling produces high coherence (less noise contamination) between pressure and seismometer signals, especially for the horizontal seismometers. In the course of similar shallow water OBS experiments in 1986–88, Trevorrow et al. (1989a) found that it was necessary to bury the seismometer housing in the surficial sediments and that the housing should be neutral density in the sediments. This negates the effects of near-bottom currents and ensures that the seismome-

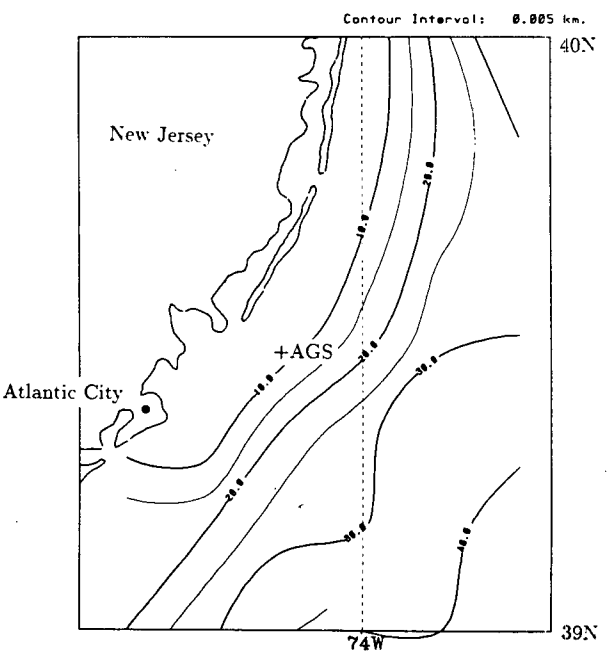

FIG. 1. Map of the New Jersey Shelf area showing the AGS site.

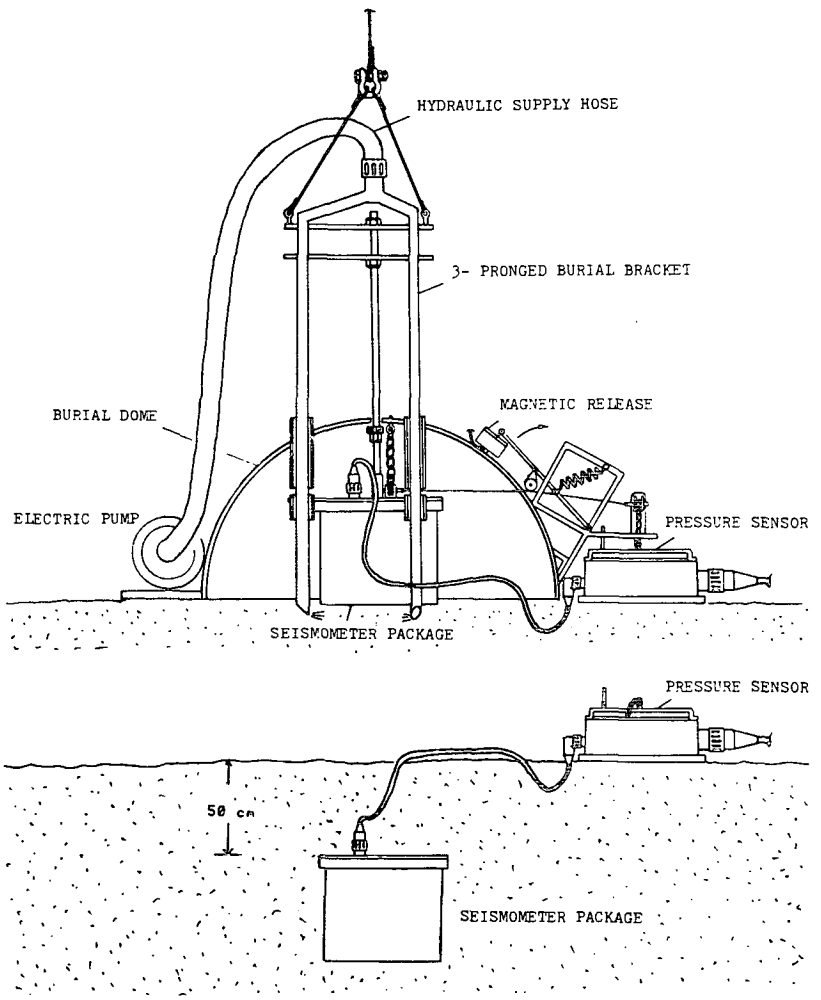

FIG. 2. (a) Apparatus for burial of the seismometer housing in the seabed sediments. (b) Buried seismometer housing.

ters follow the sediment motions exactly. Also, a buried instrument is less susceptible to storm forces and physical damage. The burial operation is more difficult to implement than a simple mooring, but well worth the effort given the improvement in data quality.

A hydraulic jet burial system was developed for this purpose (Fig. 2a). The burial system consists of a three pronged burial bracket that holds the seismometer housing. The pressure sensor housing is mounted outside the burial dome and remains on the seabed during data collection. A vertical rod keeps the pressure sensor housing aligned with the dome and therefore with the seismometers during burial. This is of paramount importance because the compass is mounted in the pressure housing to avoid magnetic interactions with seismometers. When the dome pulls off, the sensors remain aligned and so error in the heading is estimated to be less than $\pm 10°$. The directional distribution relative to the heading is not affected. Directional headings and wind conditions are measured using the ships meteorological equipment, which corrects for local magnetic declination. These and the measured sea states can be found in Table 1. The OBS headings are also corrected for local magnetic declination.

The seismometer unit is buried in the sediment to 0.5 m using seawater pumped at high pressure through the prongs of the burial bracket (Fig. 2b). Water jets at the tips liquify the sediment allowing the instrument to sink of its own weight. An electromagnetic release mechanism, controlled from the ship, releases the instruments from the burial dome, which is then brought back up to the ship. Using tiltmeters fixed inside the seismometer housing, it was possible to determine if the unit was level. If the tilt was greater than 10°, or the compass took an erratic swing as the dome was pulled up, the package was hauled up to the ship and redeployed.

Typically one to five attempts were necessary to successfully implant the seismometer housing. One major problem encountered in these experiments was that

TABLE 1. Environmental conditions and instrument response.

Dataset	Date (July 88)	Wind speed ($m\ s^{-1}$)	Wind direction (deg from)	Heading (deg radial)	H_s (m)	T_s (sec)	Propagation direction (deg toward)
305A	9	3–5	195	110	0.40	7.6	340
305B	10	6–7	200	110	0.53	6.9	355
301B	10	6–7	200	241	0.54	6.1–7.6	360–340

the ship needed to remain stationary relative to the seabed during the deployment of the instruments and also during data collection. This necessitated two or three-point mooring of the ship, which is physically difficult in rough weather. In the future, a more permanent installation could be implemented through the use of either independent surface radio-telemetry buoys or hard-wiring to shore.

The seismometer housing (aluminum alloy cylinder) contains three orthogonally (vertical, radial, and transverse) mounted seismometers (Teledyne-Geotech models S-510 or S-750) and two pendulum tiltmeters. The pressure housing is a flat aluminum cylinder and contains the compass (Aanderaa model 1248), power supply conditioners, the pressure sensor pre-amplifier and the pressure sensor itself (InterOcean model WS200). The units are connected to the ship by a 32-conductor electromechanical cable.

Data was recorded on 9 and 10 July 1988 for typical durations of 8 hours. The analogue signals were amplified, filtered, and then recorded on 14 channel, 0.5 inch magnetic tape by TEAC FM data recorders. They were later digitized at 4 Hz. The data was then converted to frequency space and corrected for the frequency response of the instruments. The optimum averaging time (long enough to reduce spectral uncertainties, but short enough so as to not include nonstationarity effects) in general cannot be predicted a priori. The typical *stationary* time period was found to be in the range of 2 to 8 hours. A 4096-point (17 minutes) FFT with a 50 percent overlap averaging method was implemented to find the cross-power spectrum between signals. Each time segment was demeaned and multiplied by a 10 percent cosine taper window before being transformed into spectral components. Spectra shown here are averaged over 8 hours.

4. Results

Figure 3 shows the power spectra of the three signals (pressure, radial and transverse accelerations) for dataset 305B (seismometer 305, collection date: (B) 10

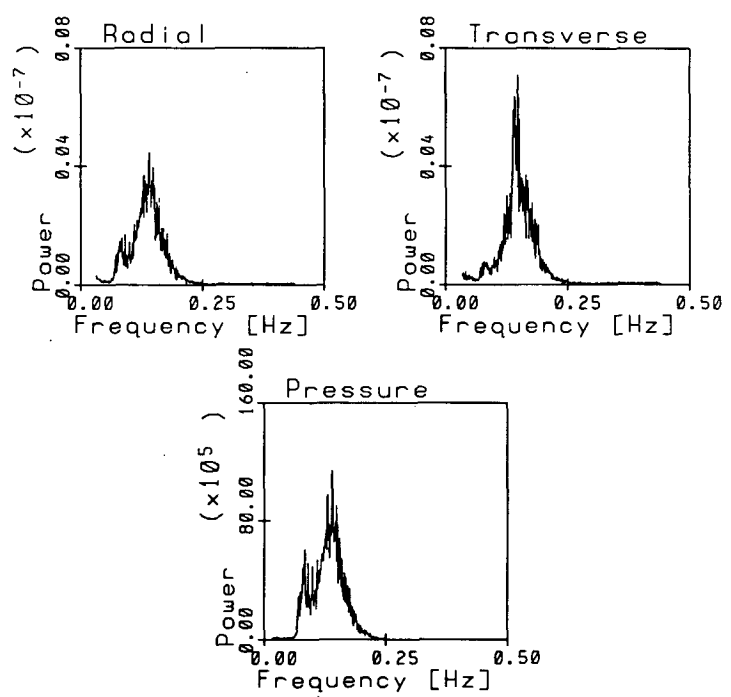

FIG. 3. Power spectra for pressure transducer, radial and transverse seismometers, unit 305B (10 July).

July, directional spectra: Fig. 6c). This figure indicates that while the radial seismometer predicts the same energy as the pressure sensor, the transverse seismometer failed to measure some of the lower frequency waves. This is better represented by plots of coherence and phase (Fig. 4). The transverse seismometer signal is not coherent with the pressure signal at frequencies less than 0.15 Hz. The transverse phase abruptly swings away from 90° (where the phase should be, in theory) at frequencies less than 0.13 Hz. This is possibly because the longer period waves propagate in a mean direction of nearly 90° from the direction of the transverse seismometer and therefore it has little energy to measure. Several other mechanisms can be considered as the cause for the deviation in the measured phase from the theoretical value. In addition to the errors in the phase versus frequency response curves of the instruments supplied by the manufacturers, we have found that if the seismometer is tilted, the phase will wander from theoretical values. The latter amounts to phase errors up to 5° while the former may be responsible for errors up to 20°. Numerical simulations have shown, however, that the directional spectrum varies appreciably only when the phase deviations of both seismometers near 90° from theory. For example, if as in Fig. 4, the phase is near 180° (about 90° from theory), but the coherence is low in the transverse direction, while the phase is closer to 270° and the coherence is high in the radial direction, the radial direction dominates. The resulting directional spectra plot is acceptable at the low frequencies where this is the case (Fig. 6a).

Figure 5 shows phase and coherence for 301B [OBS 301, (B) 10 July, Fig. 6c]. In this case, having different orientation, the transverse coherence is good, but the radial coherence is quite poor. This is probably because 301 was not coupled well (buried sufficiently) to the seafloor. Near-bottom currents were affecting the radial seismometer. As stated previously, the seismometers need to be buried 0.5 meters below the seafloor to give good coherence where they produce relatively noise-free measurements.

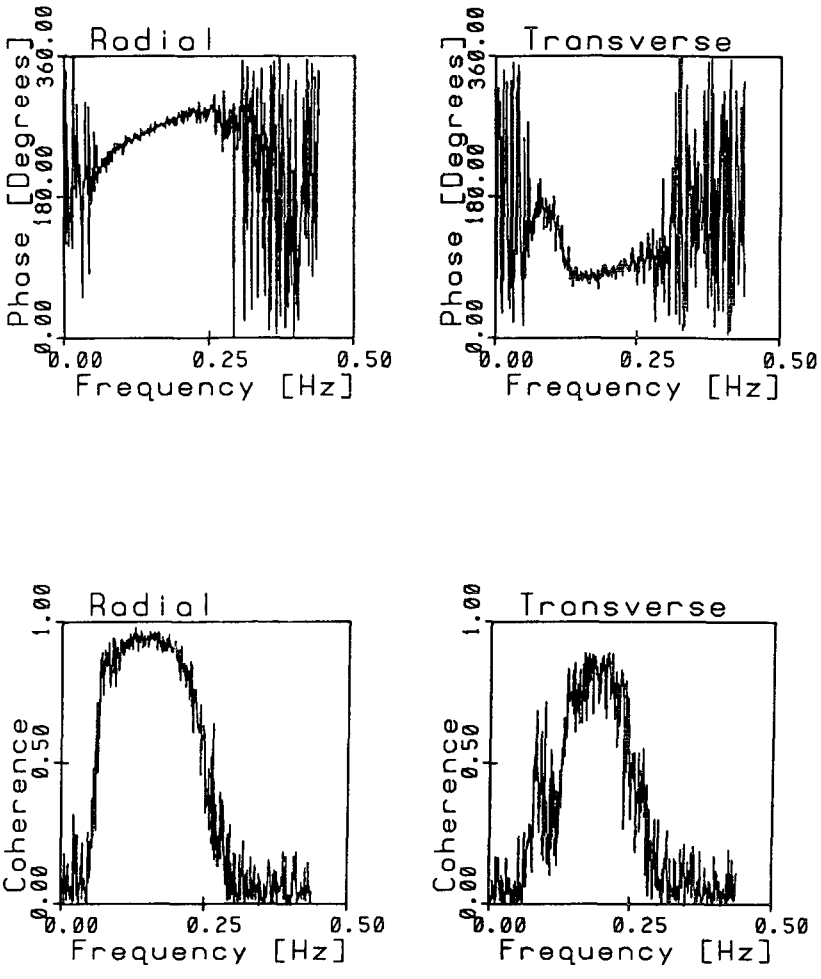

FIG. 4. Radial and transverse coherence and phases for unit 305B (10 July).

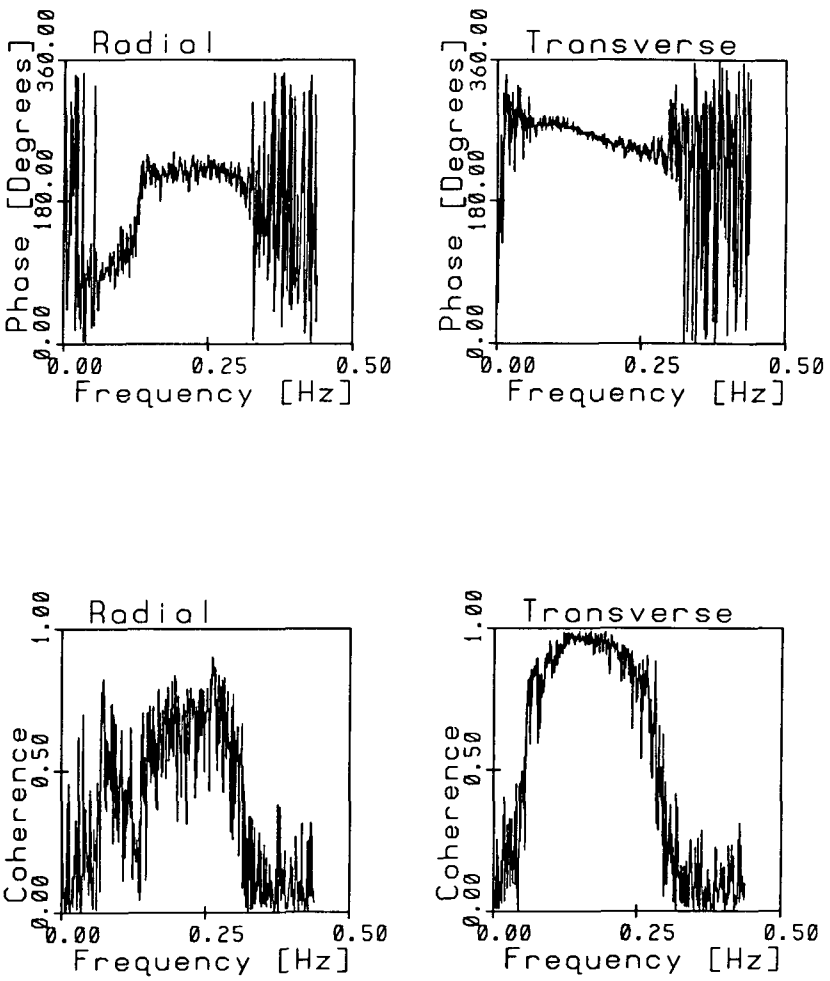

FIG. 5. As in Fig. 4 but for unit 301B (10 July).

In any case, increased coherence produces higher, more concentrated spectral peaks in the estimates. Dataset 305B (Fig. 6a) produced higher combined coherence than 301B (Fig. 6c) and the difference between estimates is noticeable though the data was collected over the same time period and approximately 400 meters apart. Set 305B shows a directional spectral estimate that has a spectral peak at 0.145 Hz (about 7 second waves) and a direction of propagation toward 355°. The half-power angular spread at the peak is 25° and expands to 35° at higher frequencies and around 60° at low frequencies. This constriction at the peak is expected (Hashimoto et al. 1987). Figure 6c, set 301B, predicts two peaks at 0.165 Hz, 360°; and 0.131 Hz, 340°. The peaks are lower and the spread wider than predicted by 305B. There is no notable constriction at the spectral peak nor the spread of energy at the low frequencies that unit 305 predicts. The half-power angular spread at the peaks are 55° and 45°, respectively, while the spread at low frequency is less than 45°. It is the authors' contention that this difference results from better coupling to the sea floor and therefore high coherence for unit 305.

A numerical simulation was conducted using a Mitsuyasu-type directional distribution. The results do not depend on the type of measurement, but only tests the principle itself. The results are the same as found by Kobune and Hashimoto (1986) and therefore will not be repeated here. The study shows that the Maximum Entropy Principle (MEP) nearly reproduces the true spectrum for unidirectional seas and for bidirectional seas with angle of separation between the two seas being greater than 60°. MLM, on the other hand, underestimates the spectral peak and shows energy in directional bands where there should be none. This *smearing* of the estimate is common for methods with directional resolution not as strong as MEP's. The experimental results show this difference between the methods. Comparing Fig. 6a (dataset 305B using MEPOBS) and Fig. 6b (same dataset using MLM) one can see that

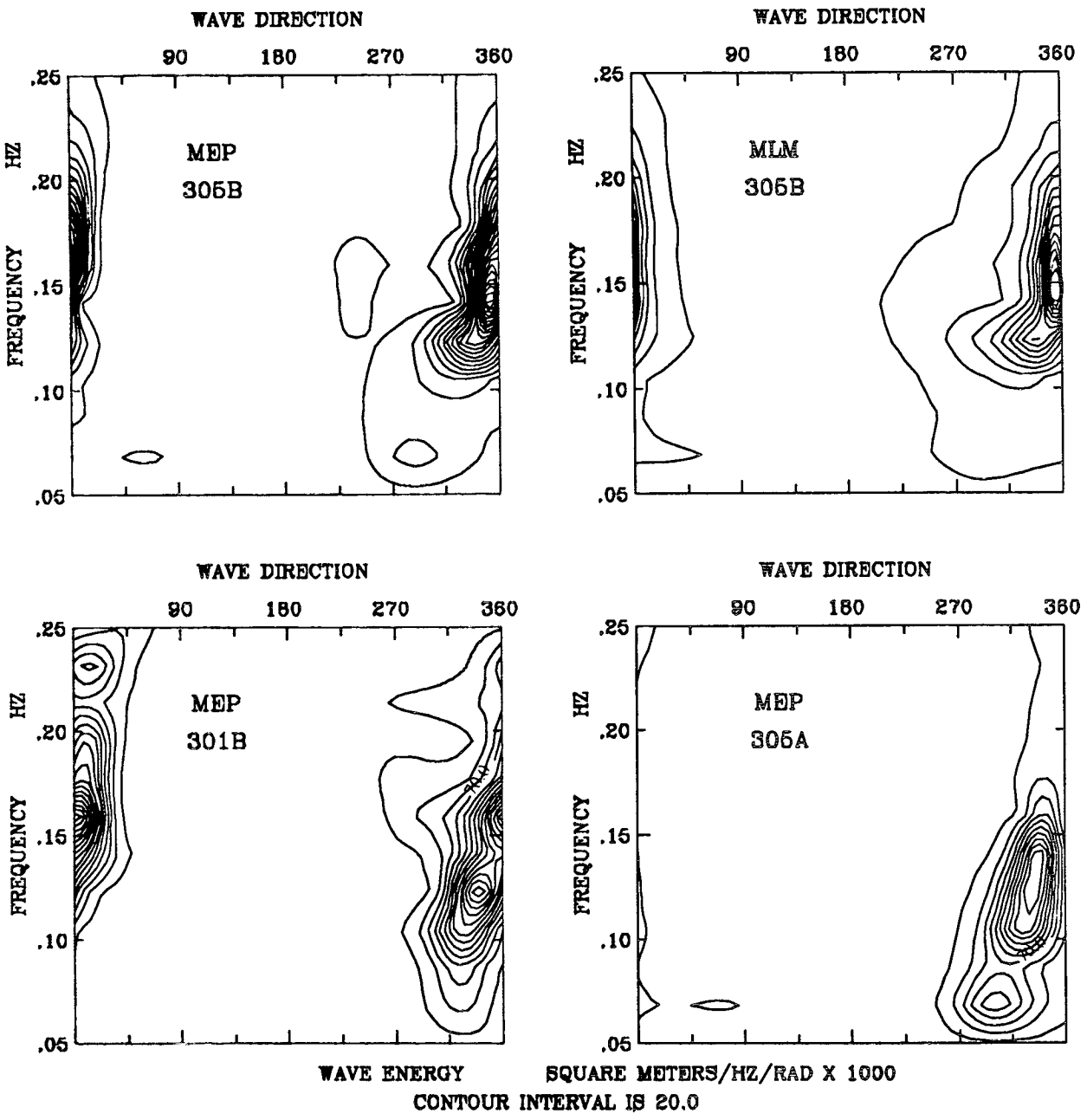

FIG. 6. Directional spectra contours: (a) dataset 305B (MEP), H_s = 0.53 meters, (b) dataset 305B (MLM), H_s = 0.53 meters, (c) dataset 301B (MEP), H_s = 0.54 meters, (d) dataset 305A (MEP), H_s = 0.40 meters.

MEPOBS produces a higher spectral peak (0.330 m^2 Hz^{-1} rad^{-1}) than MLM (0.270 m^2 Hz^{-1} rad^{-1}) and a more concentrated spectral peak (25° half-power angular spread vs 35°+). The spectral peak wave propagation direction and frequency (355°, 0.145 Hz) remain the same as does the predicted significant wave height (0.53 m). (Significant wave heights are found from the integration of the 2D power spectrum of sea surface elevation and are given in Table 1). Use of the MEP therefore produces a more detailed shape of the spectra than MLM. However, MLM still shows the peak direction and frequency while being a computationally faster technique because it does not require iterations. For most applications, the improved result by MEP will outweigh the excess cpu time.

It should be noted that the spectral peak propagation direction is not exactly 180° from the mean wind direction as would be expected (see Table 1), but is offset

by about 20° to the north. The lower frequency waves propagate toward the west (dataset 305B shows longwave energy propagating to 290°), which is to be expected. Heading error of ±10° mentioned in the previous section may be partially causing the offset. Simple refraction calculations show that waves traveling toward 15° with a period of 7 seconds will refract 5 degrees northward. The rest of the offset can be attributed to errors in estimating mean wind direction.

Figure 6d shows directional spectra for dataset 305A [unit 305, (A) 9 July]. Lack of wind on this day produced almost no energy at shorter wavelengths. The spectral peak is at 0.131 Hz and 340° azimuth. Half-power angular spread at the peak is 45° and widens to 65° at low frequencies. The significant wave height is predicted to be (0.40 m) which is significantly less than for set 305B. Dataset 301A (not shown) is similar to 305A but with less resolution yet, again due to lower coherence.

Hashimoto et al. (1987) has compared MEP with other methods and concluded that "while it measures the direction of the spectral peaks, . . . many wave properties need to be measured for a detailed analysis of the directional spectrum." The authors believe these results (specifically Fig. 6a) show that an accurate representation of the directional spectra can be found by MEPOBS given good coupling with the seabottom with respect to horizontal motions. Hashimoto et al. later state that when only three wave properties are measured, MLM and MEP are recommended for use.

5. Discussions and conclusions

The Maximum Entropy Principle utilizing measurements from an Ocean Bottom Seismometer (MEPOBS) can be used to determine the directional spectra of shallow water surface gravity waves. The directional resolution exhibited by this method is greater than that shown by MLM or any other method of analysis of a single point, three-element wave record. It is possible that better resolution or more detailed shape of the spectra is possible if an array of wave probes is used. However, for field observations, the use of arrays is financially and technically infeasible in many cases. This makes MEPOBS advantageous for many applications. For example, it is now possible to make observations of directional spectra of ocean waves using MEPOBS along much of the coastline of the United States to monitor sediment transport at relatively low cost. Ocean bottom seismometers need not be tethered to a ship as in these experiments. Radio telemetry of digital signals or hardwiring to shore are other possibilities. The latter being well suited to measure sediment transport in storm conditions. Also, the fact that directional spectra can be measured using data collected to determine another important engineering consideration, the bottom shear modulus profile, is an additional advantage. Properly buried seismometers tend to produce relatively noise-free data and are therefore well suited to give detailed shape of the directional spectra.

Due to attenuation of shorter wavelengths with depth, the method is limited to a high frequency cutoff. Where the depth is approximately half of the high-frequency wavelength, background noise is of the same magnitude as the measured accelerations and the method breaks down. The cutoff for the AGS site was 0.25 Hz, i.e. waves with periods of less than 4 seconds could not be measured. At deeper sites, only very low frequency waves can be measured, therefore, the method is only recommended for use in shallow to intermediate water depths. The method is limited to a low frequency cutoff of 0.033 Hz (30 second waves) by the seismometers used in this study. This cutoff may be extended to about 0.005 Hz (200 second waves) using broadband seismometers such as GURALP CMG-3 (Yamamoto et al. 1989).

Acknowledgments. This work was supported under U.S. Navy Office of Naval Research Contracts N00014-86-C-0198, N00014-85-C-0020, and N00014-85-G-0066 (Drs. R. Fitzgerald, and M. Orr, ONR code 1125OA). Thanks are due to Dr. R. Jacobsen (ONR code 1125GG) for his encouragement and suggestions for this work. Many thanks to the designer of the burial unit, A. Turgut. The authors would also like to thank the University of Miami's Geo-Acoustic Laboratory (C. Abbot, A. Turgut, Dr. M. Badiey, D. Goodman, and K. Ando), the crew of the University of Delaware's R/V *Cape Henlopen,* and K. Maillet for his help with NCAR plotting routines.

REFERENCES

Akaike, H., 1980: Likelihood and bayes procedure. *Bayesian Statistics,* J. M. Bernardo, M. H. DeGroot, D. U. Lindley and A. F. M. Smith, Eds., University Press, 143–166.

Borgman, L. E., 1985: Maximum-entropy and data-adaptive procedures in the investigations of ocean waves. *Maximum-Entropy and Bayesian Methods in Inverse Problems,* C. R. Smith and W. T. Grady, Eds., D. Reidel, 429–442.

Burg, J. P., 1967: Maximum entropy spectral analysis, *37th Annual International Meeting, Soc. of Explor. Geophys.,* Oklahoma City.

Capon, J., 1983: *Topics in Applied Physics* 34, *Nonlinear Methods of Spectral Analysis.* 2nd ed., S. Haykin, Ed., Springer-Verlag, Chap. 5.

Goda, Y., 1983: *Random Seas and Design of Maritime Structures.* University of Tokyo Press, 323 pp.

Hashimoto, N., K. Kobune and Y. Kameyama, 1987: Estimation of the directional spectrum using the Bayesian approach, and its application to field data analysis, Report of the Port and Harbor Research Institute, Yokosuka, Japan.

Isobe, M., K. Kondo and K. Horikawa, 1984: Extension of the MLM for estimating directional wave spectrum, *Symp. on Description and Modelling of Directional Seas,* Pap. No. A-6, 15 pp.

Jefferys, E. R., et al., 1982: Measuring directional spectra with the MLM. *Directional Wave Spectra Applications,* ASCE, 203–219.

Kobune, K., and N. Hashimoto, 1986: Estimation of directional

spectra from the maximum entropy principle, *Proc. Fifth Int. Offshore Mechanics and Arctic Engineering* (OMAE) *Symp.*, Tokyo, 80–85.

Lacoss, R. T., 1971: Data adaptive spectral analysis methods. *Geophysics,* **36**(4), 661–675.

Longuet-Higgins, M. S., D. E. Cartwright and N. D. Smith, 1963: Observations of the directional spectrum of sea waves using motions of a floating buoy. *Ocean Wave Spectra,* Prentice Hall, 111–136.

McDonough, R. N., 1983: *Topics in Applied Physics,* Vol. 34, *Nonlinear Methods of Spectral Analysis.* 2nd ed., S. Haykin, Ed., Springer-Verlag.

Mitsuyasu, H., et al., 1975: Observation of the directional spectrum of ocean waves using a cloverleaf buoy. *J. Phys. Oceanogr.*, **5**, 750–760.

Panicker, N., 1974: Review of techniques for directional wave spectra. *Ocean Waves Measurement and Analysis,* ASCE, 669–688.

Simpson, J. H., 1969: Observation of the directional characteristics of sea waves. *Geophys. J. Roy. Astron. Soc.*, **17**, 93–120.

Trevorrow, M., et al., 1988: Experimental verification of sea-bed shear modulus profile inversions using surface gravity (water) wave-induced sea-bed motion. *Geophys. J. Roy. Astron. Soc.*, **93**, 419–496.

——, et al., 1989a: Very low frequency ocean bottom seismic noise and coupling on the shallow continental shelf. *Mar. Geophys. Res.*, **11**(2), 129–152.

——, and collaborators, 1989b: Measurements of ambient seabed seismic levels below 1.0 Hz on the shallow eastern U.S. continental shelf. *J. Acoust. Soc. Am.* **86**(6), 2318–2327.

Yamamoto, T., and T. Torii, 1986: Seabed shear modulus profile inversions using surface gravity (water) wave-induced bottom motion. *Geophys. J. Roy. Astron. Soc.*, **85**, 413–431.

——, H. Koning, H. Sellmeijer and E. Van Hijum, 1978: On the response of a poroelastic bed to water waves. *J. Fluid Mech.*, **87**(1), 193–206.

——, et al., 1989: Determination of the sea-bed porosity and shear modulus profiles using a gravity wave inversion. *Geophys. J. Int.*, **98**, 173–182.